

GEMM-GS: Accelerating 3D Gaussian Splatting on Tensor Cores with GEMM-Compatible Blending

Haomin Li^{1,†}, Bowen Zhu^{1,†}, Fangxin Liu^{1,2,†,‡}, Zongwu Wang^{1,2}, Xinran Liang³, Li Jiang^{1,2,‡}, and Haibing Guan¹

1. Shanghai Jiao Tong University, 2. Shanghai Qi Zhi Institute, 3. United Imaging Intelligence Co., Ltd.
{haominli, liufangxin, ljjiang_cs}@sjtu.edu.cn

Abstract

Neural Radiance Fields (NeRF) enables 3D scene reconstruction from several 2D images but incurs high rendering latency via its point-sampling design. 3D Gaussian Splatting (3DGS) improves on NeRF with explicit scene representation and an optimized pipeline yet still fails to meet practical real-time demands. Existing acceleration works overlook the evolving Tensor Cores of modern GPUs because 3DGS pipeline lacks General Matrix Multiplication (GEMM) operations. This paper proposes GEMM-GS, an acceleration approach utilizing tensor cores on GPUs via GEMM-friendly blending transformation. It equivalently reformulates the 3DGS blending process into a GEMM-compatible form to utilize Tensor Cores. A high-performance CUDA kernel is designed, integrating a three-stage double-buffered pipeline that overlaps computation and memory access. Extensive experiments show that GEMM-GS achieves 1.42× speedup over vanilla 3DGS and provides an additional 1.47× speedup on average when combining with existing acceleration approaches. Code is released at <https://github.com/shieldforever/GEMM-GS>.

ACM Reference Format:

Haomin Li^{1,†}, Bowen Zhu^{1,†}, Fangxin Liu^{1,2,†,‡}, Zongwu Wang^{1,2}, Xinran Liang³, Li Jiang^{1,2,‡}, and Haibing Guan¹. 2026. GEMM-GS: Accelerating 3D Gaussian Splatting on Tensor Cores with GEMM-Compatible Blending. In *63rd ACM/IEEE Design Automation Conference (DAC '26)*, July 26–29, 2026, Long Beach, CA, USA. ACM, New York, NY, USA, 7 pages. <https://doi.org/10.1145/3770743.3803899>

1 Introduction

Neural rendering [19] has emerged as a transformative approach in bridging computer graphics and vision, leveraging differentiable rendering to reconstruct photo-realistic images and videos with exceptional fidelity. Early neural rendering techniques, such as Neural Radiance Fields (NeRF), marked a significant departure from traditional methods reliant on 3D grids and voxels. By harnessing the generalization capabilities of neural networks, NeRF implicitly reconstructs 3D scenes from a sparse set of 2D images, enabling

[†] These authors contributed equally to the paper. [‡] Corresponding authors. This work was partially supported by the National Key Research and Development Program of China (2024YFE0204300), National Natural Science Foundation of China (Grant No.62402311), Natural Science Foundation of Shanghai (Grant No.24ZR1433700), and Key Research and Development Program of Shanghai (25LN3201200).



This work is licensed under a Creative Commons Attribution 4.0 International License. DAC '26, Long Beach, CA, USA
© 2026 Copyright held by the owner/author(s).
ACM ISBN 979-8-4007-2254-7/2026/07
<https://doi.org/10.1145/3770743.3803899>

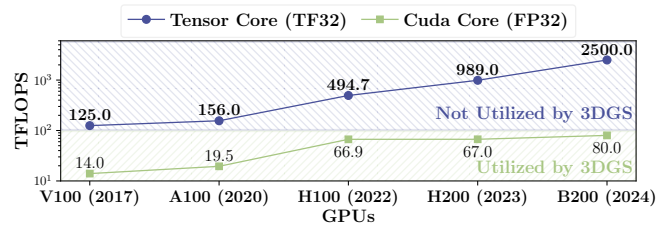


Figure 1: Computing Power Breakdown of modern GPUs utilized by 3D Gaussian Splatting. Data is collected from the data sheets of the GPU products [22–26].

high-quality rendering from novel viewpoints. This makes NeRF particularly valuable for applications like augmented reality (AR), virtual reality (VR), and 3D reconstruction [29–31, 33]. However, NeRF’s sampling-point-based design requires over a million model inferences per image, resulting in significant rendering latency that hinders real-time performance.

Recently, 3D Gaussian Splatting (3DGS) [10] has gained prominence as a highly efficient neural rendering technique. 3DGS models the scenes with parametric point clouds of differentiable 3D Gaussian primitives. By employing explicit scene representations and a well-designed rendering pipeline, 3DGS delivers better rendering quality and lower latency compared to NeRF-based methods. Therefore, 3DGS has emerged as a leading method for 3D reconstruction and differentiable rendering, widely adopted across the field.

Despite its advancements, 3DGS falls short of real-time performance required for practical applications. To be specific, as the scale and resolution of images increase, both the number of Gaussians and the size of each Gaussian grow. At the hardware level, some domain specific architectures (DSAs) have been proposed to accelerate the rendering process, but these involve significant design and tape-out costs [5, 12, 14, 16, 17, 32]. In addition, the DSAs are hard to adapt to various optimization approaches. At the software level, some works [3, 6, 13, 27] adopt mature quantization or pruning methods to reduce storage cost. For example, LightGaussian [3] adopts Gaussian pruning to reduce the huge number of Gaussians in the models and vector quantization to compress the attributes of Gaussians. However, these methods mainly focus on storage reduction, but have not yielded significant performance improvements. Some other software efforts [4, 7, 28] focus on optimizing GPU implementation, achieving performance gains by improving the precision of intersection detection during the preprocessing stage to reduce redundant duplication of Gaussians.

However, existing software optimization methods overlook the evolutionary characteristics of modern GPUs, namely the increasingly powerful TensorCores capable of efficiently performing general matrix multiplication (GEMM). That’s because the rendering

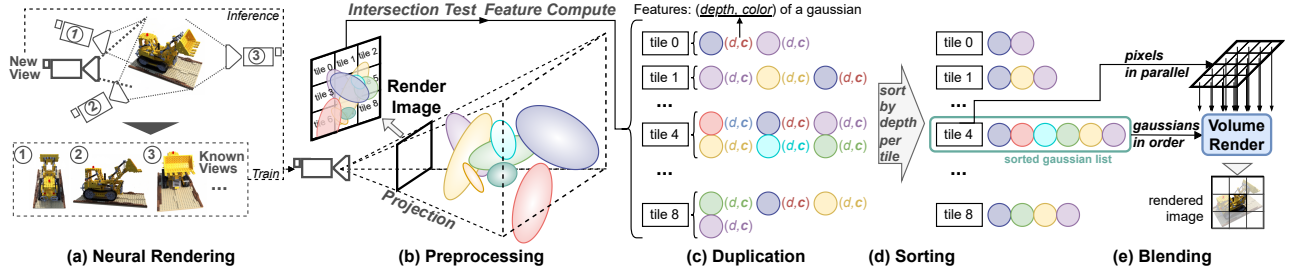


Figure 2: Neural Rendering and Process of 3DGS [10]. (a) Neural rendering (process of novel view synthesis). 3DGS consists of three stages. (b) Stage 1: Preprocessing. Gaussians are projected onto the render image and intersection test is performed to relating projected Gaussians and tiles. Gaussians’ features are also computed, including depth d and color c . (c) Stage 2: Duplication. Each Gaussian is duplicated according to the number of tiles it intersects with. (d) Stage 3: Sorting. Gaussians in each tile are sorted by depth d . (e) Stage 4: Blending. The pixels in one tile are rendered by volume rendering in parallel, with the same sorted Gaussian list.

pipeline of 3DGS contains few GEMM-style operations, resulting in idle Tensor Cores on GPUs. As shown in Figure ??, starting from the Volta architecture, the computing power of GPU Tensor Cores has become increasingly stronger. Therefore, how to design a GEMM-friendly 3DGS rendering pipeline to fully utilize the powerful computing capabilities of Tensor Cores is the key to improving 3DGS performance.

To this end, this paper proposes GEMM-GS, an acceleration approach utilizing tensor cores on GPUs via GEMM-friendly blending transformation. We transform the conventional 3DGS blending process into a GEMM-style formulation equivalently, leveraging the powerful tensor cores in modern GPUs for acceleration. To fully utilize the computing resources, we develop a well-designed blending kernel in CUDA. Based on the asynchronous memory copy technique, the kernel is designed as a three-stage pipeline with double buffer, well overlapping the computation and memory access. The results demonstrate that GEMM-GS delivers 1.42× speedup over the vanilla 3DGS implementation on average. It is worth noting that our approach is orthogonal to existing acceleration methods, and can achieve an additional 1.47× speedup over them. Our contributions are summarized as follows:

- We propose an equivalent transformation to reformulate the 3DGS blending process into a GEMM-compatible form, enabling the effective utilization of idle Tensor Cores on GPUs.
- We develop a CUDA kernel to implement the transformed blending process. The kernel adopts a three-stage double-buffered pipeline with asynchronous memory copy, fully overlapping Tensor Core computation and memory access.
- Evaluations demonstrate that GEMM-GS achieves an average 1.42× speedup over vanilla 3DGS and an additional 1.47× speedup when combined with existing methods. Moreover, GEMM-GS is directly deployable on commodity GPUs without hardware modification, ensuring low adoption cost and real-world applicability.

2 Background

2.1 3D Gaussian Splatting

3D Gaussian Splatting (3DGS) represents a scene using Gaussian ellipsoids and renders it in a tile-by-tile fashion. As illustrated in

Figure 2, the rendering pipeline consists of four stages: preprocessing, duplication, sorting, and blending. **(a) Preprocessing:** Given a camera pose, 3D Gaussians within the view frustum are projected onto the 2D image plane (from ellipsoids to ellipses). The 2D screen is divided into tiles (e.g., 16×16 pixels) based on the target resolution and tile size. Intersection detection identifies which Gaussians contribute to each tile. For each projected Gaussian, depth d and RGB color c are computed for use in subsequent stages. **(b) Duplication:** To facilitate parallel blending, each Gaussian is duplicated according to the number of tiles it overlaps. Specifically, each copy is assigned a tile index, which is concatenated with the depth value to ensure that Gaussians corresponding to the same tile are gathered after sorting. **(c) Sorting:** Each tile may intersect multiple Gaussians, with closer Gaussians occluding those farther away. To ensure correct rendering, Gaussians are sorted by depth d . GPU implementations typically employ radix sort [10] to exploit CUDA core parallelism, producing a sorted list of Gaussians for each tile. **(d) Blending:** Blending iterates through the sorted Gaussians for each tile, processing all pixels in parallel. For each Gaussian \mathcal{G}_i and pixel p_j , the opacity α_{ij} and the corresponding color contribution to p_j are computed according to standard volume rendering operations:

$$C_j = \sum_{i=1}^N T_i \alpha_{ij} c_i, \quad T_i = \prod_{k=1}^{i-1} (1 - \alpha_{kj}), \quad (1)$$

where C_j is the rendered color of pixel p_j , and T_i represents the accumulated transmittance up to Gaussian i .

As shown in Algorithm 1, rendering a 16×16 tile is assigned to a thread block of 256 threads, with each thread handling one pixel. For Gaussians stored in global memory, the thread block processes them in batches, loading one batch into shared memory at a time. Each thread iterates over the Gaussian attributes to compute the pixel color according to Eq.(1). This tile-based organization enables coalesced memory accesses and efficient use of shared memory, reducing memory bandwidth pressure and improving throughput.

2.2 3DGS GPU Acceleration

To improve the rendering speed of 3DGS models, existing acceleration approaches can be broadly categorized into compression-based and preprocessing-based methods.

Algorithm 1: Blending Process in Vanilla 3DGS [10].

Data: Index list of sorted projected Gaussians \mathcal{G} overlapping with current tile, batch size b
Result: Rendered Color C_j s of pixels in current tile

```

1 for each batch ( $b$  Gaussians)  $\subset \mathcal{G}$  do
2   /***** Prepare Data *****/
3   for each Gaussian  $\mathcal{G}_i$  in current batch parallel do
4     Fetch data of Gaussian  $\mathcal{G}_i$ :
5     projected coordinates:  $(x_{g_i}, y_{g_i})$ 
6     covariance matrix:  $\Sigma_i = \begin{bmatrix} A_i & B_i \\ B_i & C_i \end{bmatrix}$ 
7     opacity weight and RGB color:  $o_i$  and  $\mathbf{c}_i$ 
8   end
9   /***** Volume Render *****/
10  for each Gaussian  $\mathcal{G}_i$  in current batch do
11    for each pixel  $p_j$  in current tile parallel do
12       $\mathbf{x}_{g_i} \leftarrow [x_{g_i} - x_{p_j} \quad y_{g_i} - y_{p_j}]^T$ 
13       $\alpha_{ij} \leftarrow o_i \times \exp(-\frac{1}{2} \mathbf{x}_{g_i}^T \Sigma_i^{-1} \mathbf{x}_{g_i})$ 
14      if  $\alpha_{ij} \leq \frac{1}{255}$  then
15        | skip to next Gaussian //  $\alpha$ -skipping [10]
16      end
17       $T_j \leftarrow T_j \times (1 - \alpha_{ij})$ 
18      if  $T_j \leq 0$  then
19        | stop rendering  $p_j$  // early terminate[19]
20      end
21       $C_j \leftarrow C_j + \mathbf{c}_i \alpha_{ij} T_j$ 
22    end
23  end
24 end

```

Compression-based approaches aim to reduce the memory footprint of Gaussian representations. Two common techniques are pruning, which reduces the number of Gaussians based on importance metrics [8, 18], and vector quantization (VQ), which represents the attribute vectors of a large number of Gaussians using a small set of cluster centroids [2, 20, 21]. Some works, such as LightGaussian [3], combine pruning and VQ to achieve further storage reduction [6, 13, 27]. However, these approaches typically require retraining the model to restore rendering quality.

Preprocessing-based approaches focus on optimizing Gaussian intersection tests to avoid redundant processing, without modifying the underlying 3DGS models. FlashGS [4] employs a precise redundancy elimination algorithm with opacity skipping. StopThePop [28] introduces a tile-based culling strategy similar to FlashGS. Speedy-Splat [7] proposes the SnugBox algorithm, which constructs tight bounding boxes around each Gaussian and identifies the exact set of intersected tiles. These methods are lossless and do not require retraining or model modification.

2.3 Analysis and Motivation

We first profile 3DGS rendering latency across scenes from three datasets [1, 9, 11] on an NVIDIA A100 GPU (Figure 3). The results show that the blending stage contributes nearly 70% of the total

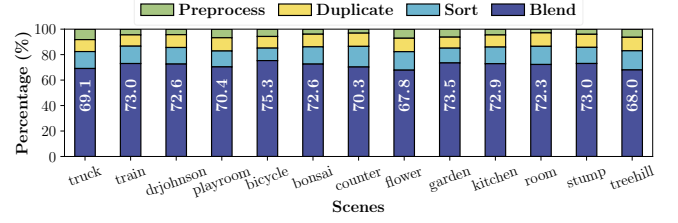


Figure 3: Rendering Latency Breakdown of 3DGS. The scenes for rendering are from three datasets: Tank&Temples [11], Deep Blending [9], and Mip-NeRF 360 [1].

rendering time, making it the primary performance bottleneck. At the same time, modern GPUs feature increasingly powerful Tensor Cores optimized for GEMM-based computations. As illustrated in Figure 1, the theoretical FLOPS of Tensor Cores on the latest GPUs can exceed 30 times that of CUDA cores. However, the conventional 3DGS pipeline contains very few GEMM-style operations, leaving these resources largely idle and representing a substantial opportunity for acceleration.

These observations motivate our primary optimization target: transforming the blending stage into a GEMM-compatible pipeline to leverage the idle Tensor Cores. To this end, we propose **GEMM-GS**, which constructs a GEMM-compatible computation pipeline by applying an equivalent transformation to the blending stage and implements a high-performance CUDA kernel for accelerated Gaussian blending. Our approach is orthogonal to existing GPU acceleration methods and provides a plug-and-play tensor-based computation framework, enabling further acceleration of various state-of-the-art 3DGS implementations.

3 GEMM-GS Design and Implementation

The blending stage dominates the computational cost of 3DGS. To exploit Tensor Cores, GEMM-GS reformulates the opacity computation (α) into a GEMM-compatible form and designs a high-performance CUDA kernel that fully leverages the GPU memory hierarchy and parallel execution resources.

3.1 Calculation Form of α 's Exponential

In 3DGS, the opacity α_{ij} of a Gaussian \mathcal{G}_i at pixel p_j is computed as:

$$\alpha_{ij} = o_i \times e^{-\frac{1}{2} \mathbf{x}_{g_i}^T \Sigma_i^{-1} \mathbf{x}_{g_i}} \quad (2)$$

where $\mathbf{x}_{g_i} = [\Delta x_{ij} \quad \Delta y_{ij}]^T = [x_{g_i} - x_{p_j} \quad y_{g_i} - y_{p_j}]^T$, i.e., the vector from the projected coordinate of Gaussian g_i (x_{g_i}, y_{g_i}) to the coordinate of the current pixel (x_{p_j}, y_{p_j}). $\Sigma_i = \begin{bmatrix} A_i & B_i \\ B_i & C_i \end{bmatrix}$ is the covariance matrix of g_i .

Thus, the exponential term in Eq.(2) is expanded as

$$\text{power}_{ij} = -\frac{1}{2} A_i \Delta x_{ij}^2 - B_i \Delta x_{ij} \Delta y_{ij} - \frac{1}{2} C_i \Delta y_{ij}^2 \quad (3)$$

This formulation involves element-wise quadratic terms, which cannot be directly expressed as a matrix multiplication. As a result, the blending stage cannot natively benefit from Tensor Cores, leading to low compute efficiency on modern GPUs. GEMM-GS addresses this by transforming the computation into a GEMM-compatible representation, enabling effective Tensor Core acceleration.

3.2 Transformation based on Intra-Tile Coordinates

To enable Tensor Core utilization, we reformulate the opacity computation in the blending stage into a dot-product form. The key idea is to exploit intra-tile relative coordinates so that the quadratic power term can be expressed as a linear dot product, which is then amenable to batched matrix multiplications. For each tile, we select a reference pixel p_c (e.g., the center pixel) with coordinates (x_c, y_c) . The coordinates of any pixel p_j in the tile can be expressed as:

$$(x_{p_j}, y_{p_j}) = (x_c - \bar{x}_{p_j}, y_c - \bar{y}_{p_j}), \quad (4)$$

where $(\bar{x}_{p_j}, \bar{y}_{p_j})$ are the intra-tile relative coordinates of p_j with respect to p_c . Accordingly, the coordinate differences between a Gaussian \mathcal{G}_i and pixel p_j become:

$$\Delta x_{ij} = (x_{g_i} - x_c) + \bar{x}_{p_j}, \quad \Delta y_{ij} = (y_{g_i} - y_c) + \bar{y}_{p_j} \quad (5)$$

We let \hat{x}_{g_i} and \hat{y}_{g_i} to denote the blue parts $x_{g_i} - x_c$ and $y_{g_i} - y_c$, which are the coordinate differences between Gaussian \mathcal{G}_i and the reference pixel p_c . These pairs of values $(\hat{x}_{g_i}, \hat{y}_{g_i})$ s are constant for all pixels in a tile for a given Gaussian, requiring computation only once per tile.

Substituting these terms into Eq.(3), the quadratic form can be reorganized as:

$$\begin{aligned} power_{ij} &= -\frac{1}{2}A_i(\hat{x}_{g_i} + \bar{x}_{p_j})^2 - B_i(\hat{x}_{g_i} + \bar{x}_{p_j})(\hat{y}_{g_i} + \bar{y}_{p_j}) \\ &\quad - \frac{1}{2}C_i(\hat{y}_{g_i} + \bar{y}_{p_j})^2 \\ &= \begin{bmatrix} -\frac{1}{2}A_i \\ -\frac{1}{2}C_i \\ -B_i \\ -A_i\hat{x}_{g_i} - B_i\hat{y}_{g_i} \\ -C_i\hat{y}_{g_i} - B_i\hat{x}_{g_i} \\ -\frac{1}{2}A_i\hat{x}_{g_i}^2 - \frac{1}{2}C_i\hat{y}_{g_i}^2 - B_i\hat{x}_{g_i}\hat{y}_{g_i} \end{bmatrix}^T \cdot \begin{bmatrix} \bar{x}_{p_j}^2 \\ \bar{y}_{p_j}^2 \\ \bar{x}_{p_j}\bar{y}_{p_j} \\ \bar{x}_{p_j} \\ \bar{y}_{p_j} \\ 1 \end{bmatrix} \\ &= \vec{v}_{g_i} \cdot \vec{v}_{p_j} \end{aligned} \quad (6)$$

where $\vec{v}_{g_i} \in \mathbb{R}^6$ is a vector determined by Gaussian parameters (A_i, B_i, C_i) and offsets $(\hat{x}_{g_i}, \hat{y}_{g_i})$, and $\vec{v}_{p_j} \in \mathbb{R}^6$ encodes intra-tile relative coordinate terms for pixel p_j . Notably, the \vec{v}_{p_j} vectors depend only on intra-tile relative coordinates and constant terms, making them independent of specific Gaussians or tile positions. Hence, \vec{v}_{p_j} for all pixels in a tile can be precomputed once offline, stored in global memory, and reused throughout the rendering process. In contrast, \vec{v}_{g_i} must be computed once per Gaussian per tile, as it incorporates both Gaussian parameters and relative offsets $(\hat{x}_{g_i}, \hat{y}_{g_i})$.

This reformulation converts the blending stage into a set of six-dimensional dot products, which can be naturally expressed as matrix multiplications. Specifically, a matrix composed of \vec{v}_{g_i} vectors for multiple Gaussians is multiplied by a matrix of \vec{v}_{p_j} vectors for all pixels in a tile, enabling direct mapping to high-throughput GEMM operations on Tensor Cores.

3.3 GEMM-compatible Blending

Building on the intra-tile coordinate transformation, we formulate the computation of multiple $power_{ij}$ values as a batched matrix multiplication. This converts the collection of six-dimensional dot

Algorithm 2: GEMM-compatible Blending Process.

Data: Index list of sorted projected Gaussians \mathcal{G} overlapping with current tile, batch size b , offline-computed matrix \mathbf{M}_p

Result: Rendered Color \mathbf{C}_j s of pixels in current tile

```

1 for each batch ( $b$  Gaussians)  $\subset \mathcal{G}$  do
2     /***** Prepare Data *****/
3     Same as Line 3-8 in Algorithm 1
4     /***** Construct Matrix *****/
5     for each Gaussian  $\mathcal{G}_i$  in current batch parallel do
6          $\vec{v}_{g_i} \leftarrow [ -\frac{1}{2}A_i, -\frac{1}{2}C_i, -B_i, -A_i\hat{x}_{g_i} - B_i\hat{y}_{g_i},$ 
7              $-C_i\hat{y}_{g_i} - B_i\hat{x}_{g_i}, -\frac{1}{2}A_i\hat{x}_{g_i}^2 - \frac{1}{2}C_i\hat{y}_{g_i}^2 - B_i\hat{x}_{g_i}\hat{y}_{g_i} ]$  // Eq 6
8     end
9      $\mathbf{M}_g \leftarrow [ \vec{v}_{g_0}^T, \vec{v}_{g_1}^T, \dots, \vec{v}_{g_i}^T, \dots, \vec{v}_{g_b}^T ]^T$  // Eq 7
10    /** GEMM-Compatible Volume Render **/
11     $\mathbf{M}_{power} \leftarrow \mathbf{M}_g \cdot \mathbf{M}_p$  // Eq 8
12    for each Gaussian  $\mathcal{G}_i$  in current batch do
13        for each pixel  $p_j$  in current tile parallel do
14             $\alpha_{ij} \leftarrow o_i \times \exp(\mathbf{M}_{power}[i][j])$ 
15            Same as Line 14-21 in Algorithm 1
16        end
17    end

```

products into a single GEMM operation, allowing efficient execution on GPU Tensor Cores for 3DGS acceleration.

For a 16×16 tile (256 pixels) and a batch of 256 Gaussians—typical in 3DGS rendering [10]—we construct a 256×6 Gaussian matrix \mathbf{M}_g and a 256×6 pixel matrix \mathbf{M}_p based on Eq. (6):

$$\begin{aligned} \mathbf{M}_g &= [\vec{v}_{g_0}^T \quad \vec{v}_{g_1}^T \quad \dots \quad \vec{v}_{g_i}^T \quad \dots \quad \vec{v}_{g_{255}}^T] \\ \mathbf{M}_p &= [\vec{v}_{p_0} \quad \vec{v}_{p_1} \quad \dots \quad \vec{v}_{p_i} \quad \dots \quad \vec{v}_{p_{255}}] \end{aligned} \quad (7)$$

The power values are computed via matrix multiplication:

$$\mathbf{M}_{power} = \mathbf{M}_g \cdot \mathbf{M}_p \quad (8)$$

where \mathbf{M}_{power} is a 256×64 matrix containing all $power_{ij}$ values for Gaussian-pixel pairs within the tile. As discussed in Section 3.2, \mathbf{M}_p remains identical across tiles due to fixed intra-tile coordinates, enabling offline precomputation and reuse with negligible overhead.

Algorithm 2 summarizes the blending procedure. In contrast to vanilla 3DGS blending (Algorithm 1), which evaluates $power_{ij}$ per pixel individually, our method directly consumes the offline-precomputed \mathbf{M}_p . For each tile, the steps are: 1) Fetch Gaussian attributes $(A_i, B_i, C_i, x_{g_i}, y_{g_i})$ for the current Gaussian batch. 2) Compute \vec{v}_{g_i} for each Gaussian \mathcal{G}_i using dx_{ic} and \hat{y}_{g_i} , forming \mathbf{M}_g . 3) Perform matrix multiplication (Eq.(8)) to obtain \mathbf{M}_{power} . 4) Execute volume rendering, computing α_{ij} using exponentials of \mathbf{M}_{power} values, consistent with Algorithm 1.

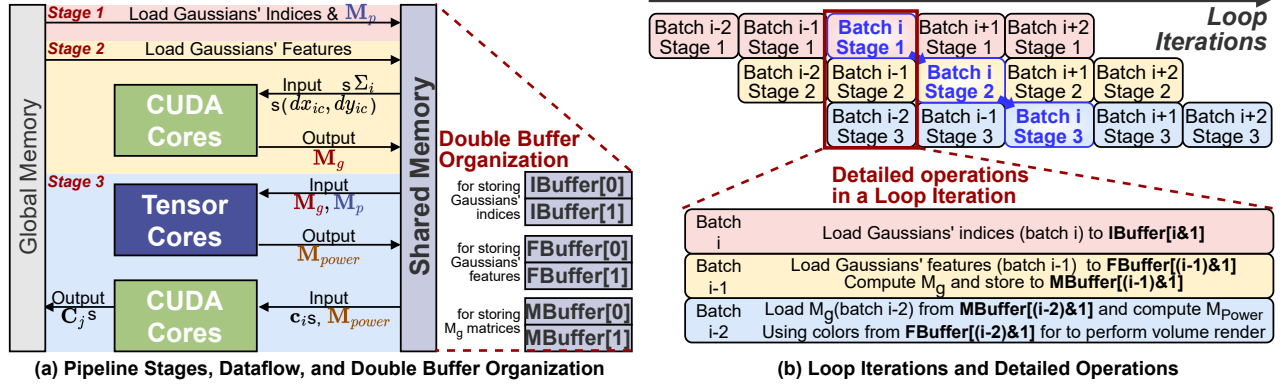


Figure 4: High-Performance GPU Kernel Design and Implementation. (a) Dataflow of 3-stage pipeline configured with double buffer. (b) Execution timing of loop iterations and detailed operations in a single iteration.

Table 1: 3DGS Workloads Statics.

| Datasets | Scenes | Resolution | #Gaussians |
|--|--|--------------------------|------------------|
| Tank & Temples (Outdoor) [11] | Train Truck | 980 × 545 979 × 546 | 1.09M 2.06M |
| Deep Blending (Indoor) [9] | Playroom Drjohnson | 1264 × 832 1332 × 876 | 1.85M 3.07M |
| Mip-NeRF 360 (5 outdoors, 4 indoors) [1] | bicycle, bonsai, counter, flowers, garden, kitchen, room, stump, treehill | around 1060 × 1600 | 1.04M ~ 4.74M |

3.4 GPU Implementation

Following the vanilla implementation [10], we assign a thread block of 256 threads to render each 16×16 tile and process the sorted Gaussian list with a batch size of 256.

Three-Stage Pipeline. To overlap latency and reduce synchronization overhead, we design a three-stage pipeline, illustrated in Figure 4(a): Stage 1: Load Gaussian indices into shared memory. Stage 2: Each thread fetches the attributes of one Gaussian according to its index (as in line 4 of Algorithm 2), and collaboratively constructs M_g . Each thread computes one $\vec{v}g_i$ vector, forming the rows of M_g . Stage 3: Perform matrix multiplication between the preloaded M_p and the constructed M_g to obtain M_{power} , followed by volume rendering.

Mini-batch Design with PTX-based GEMM Instruction. Due to limited shared memory, Stage 3 adopts a mini-batch design. In each iteration, a 16×8 submatrix of M_g is multiplied with M_p . The multiplication is executed via four rounds of warp-level `mma(m16n8k8)` PTX instructions¹, where each thread block consists of 8 warps (32 threads per warp). Thus, $8 \times 4 = 32$ warp-level calls complete an effective `m256n16k8` multiplication. This partitioning confines synchronization to the warp level, eliminating costly thread block barriers.

Double Buffer Organization. We employ double buffering for Gaussian indices, features, and the matrix M_g , as illustrated in

Figure 4(b). Double buffering of indices enables the use of asynchronous memory copy², introduced in the Ampere architecture, to overlap data transfer with computation. Similarly, double buffering of features and M_g prevents synchronization stalls between Stage 2 and Stage 3. This design minimizes global memory traffic, ensuring sustained tensor-core utilization.

4 Evaluation

4.1 Methodology

Workloads and Datasets. We evaluate 3DGS on three widely-used real-world datasets: Tank & Temples [11], Deep Blending [9], and Mip-NeRF 360 [1]. Each scene is trained for 30K iterations using the official 3DGS pipeline. In total, we evaluate across 13 scenes (workloads), with dataset statistics summarized in Table 1.

Implementation and Baselines. We implement our design on 2 types of NVIDIA GPUs: A100 and H100. We use CUDA events to delay the forward rendering process within the forward function. For each scene, we iterate through rendering the entire test dataset 10 times, record the latency, and take the average. Apart from the Vanilla 3DGS implementation [10], we select several representative 3DGS acceleration as baselines. Preprocess Optimization Methods: FlashGS [4], StopThePop [28], and Speedy-Splat [7]. Compression Methods: LightGaussian [3] and c3dgs [13]. We compare the latency of these baseline designs with the latency after integrating the proposed GEMM-GS into these designs.

4.2 Performance Comparison

Table 2 and Figure 5 compares the latency between baseline methods and our GEMM-GS. Compared to the vanilla 3DGS, GEMM-GS achieves 1.42× and 1.37× speedup on A100 and H100, respectively. Such improvements are due to utilization of powerful tensor cores on GPUs and efficient pipeline kernel design. Furthermore, we integrate GEMM-GS with several preprocess optimization methods. GEMM-GS provides averagely 1.19× (1.21×), 1.42× (1.33×), and 1.50× (1.44×) over FlashGS, StopThePop, and SpeedySplat on A100 (H100), demonstrating that our method is orthogonal to existing

¹ <https://docs.nvidia.com/cuda/parallel-thread-execution/index.html#warp-level-matrix-fragment-mma-1688>.

² <https://docs.nvidia.com/cuda/cuda-c-programming-guide/index.html#pipeline-primitives-interface>.

Table 2: Average image rendering latency (ms) comparison between GEMM-GS and baseline methods on an A100 GPU.

| Datasets | Tank & Temples [11] | | Deep Blending [9] | | Mip-NeRF 360 [1] | | | | | | | | |
|----------------|---------------------|--------------|-------------------|--------------|------------------|--------------|--------------|--------------|--------------|--------------|--------------|--------------|--------------|
| Scenes | truck | train | drjohnson | playroom | bicycle | bonsai | counter | flowers | garden | kitchen | room | stump | trehill |
| Vanilla 3DGS | 4.28 | 4.51 | 6.16 | 4.37 | 9.64 | 3.77 | 5.17 | 4.22 | 6.49 | 5.97 | 5.32 | 4.73 | 5.02 |
| + GEMM-GS | 2.78 | 3.01 | 4.16 | 2.86 | 6.87 | 2.7 | 3.72 | 2.99 | 4.81 | 4.33 | 3.97 | 3.47 | 3.63 |
| Speedup | 1.54× | 1.50× | 1.48× | 1.53× | 1.40× | 1.40× | 1.39× | 1.41× | 1.35× | 1.38× | 1.34× | 1.36× | 1.38× |
| FlashGS | 2.53 | 2.6 | 2.08 | 1.51 | 4.16 | 1.52 | 2.08 | 2.31 | 3.74 | 2.84 | 2.02 | 2.71 | 2.48 |
| + GEMM-GS | 2.29 | 2.15 | 1.58 | 1.23 | 3.69 | 1.27 | 1.73 | 1.93 | 3.21 | 2.39 | 1.72 | 2.28 | 2.15 |
| Speedup | 1.10× | 1.21× | 1.32× | 1.23× | 1.13× | 1.20× | 1.20× | 1.20× | 1.17× | 1.19× | 1.17× | 1.19× | 1.15× |
| StopThePop | 3.52 | 3.86 | 5.49 | 3.53 | 8.91 | 2.91 | 4.31 | 3.62 | 5.74 | 5.31 | 4.72 | 4.12 | 4.28 |
| + GEMM-GS | 2.56 | 2.67 | 3.75 | 2.23 | 6.28 | 2.016 | 3.11 | 2.63 | 4.324 | 3.83 | 3.35 | 2.928 | 3.048 |
| Speedup | 1.38× | 1.45× | 1.46× | 1.58× | 1.42× | 1.45× | 1.39× | 1.38× | 1.33× | 1.39× | 1.41× | 1.41× | 1.40× |
| Speedy-Splat | 2.83 | 2.93 | 2.85 | 2.01 | 4.7 | 1.91 | 2.5 | 2.61 | 4.16 | 3.37 | 2.31 | 2.99 | 2.82 |
| + GEMM-GS | 1.86 | 1.88 | 1.79 | 1.26 | 3.38 | 1.25 | 1.59 | 1.78 | 2.79 | 2.44 | 1.44 | 2.09 | 2.04 |
| Speedup | 1.52× | 1.56× | 1.59× | 1.60× | 1.39× | 1.53× | 1.57× | 1.47× | 1.49× | 1.38× | 1.60× | 1.43× | 1.38× |
| c3dgs | 4.3 | 4.93 | 6.22 | 4.35 | 10.85 | 4.37 | 5.92 | 4.71 | 7.83 | 7.37 | 6 | 5.53 | 6.09 |
| + GEMM-GS | 2.53 | 2.89 | 3.49 | 2.44 | 6.29 | 2.55 | 3.4 | 2.87 | 4.56 | 4.18 | 3.37 | 3.18 | 3.61 |
| Speedup | 1.70× | 1.71× | 1.78× | 1.78× | 1.72× | 1.71× | 1.74× | 1.64× | 1.72× | 1.76× | 1.78× | 1.74× | 1.69× |
| LightGaussian | 2.9 | 2.29 | 3.55 | 2.7 | 5.96 | 2.95 | 3.94 | 3.38 | 5.14 | 4.17 | 4 | 3.85 | 4.18 |
| + GEMM-GS | 1.85 | 1.51 | 2.2 | 1.68 | 3.67 | 1.88 | 2.48 | 2.18 | 3.23 | 2.62 | 2.49 | 2.47 | 2.6 |
| Speedup | 1.57× | 1.52× | 1.61× | 1.61× | 1.62× | 1.57× | 1.59× | 1.55× | 1.59× | 1.59× | 1.61× | 1.56× | 1.61× |

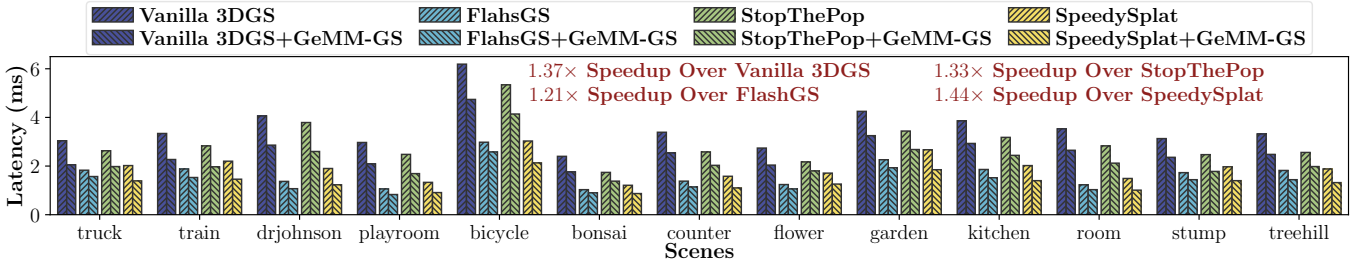


Figure 5: Average image rendering latency (ms) comparison between GEMM-GS and baseline methods on an H100 GPU.

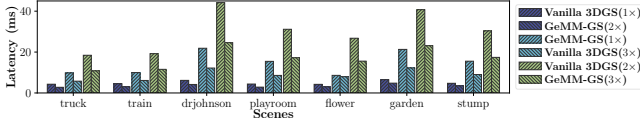


Figure 6: Average image rendering latency (ms) comparison between GEMM-GS and vanilla 3DGS with various resolution (1x, 2x, 3x).

methods and can be combined with them to achieve co-optimization for better performance. In addition, we evaluate GEMM-GS integrated with compression methods on A100. GEMM-GS achieves 1.73x and 1.58x over c3dgs and LightGaussian on average, indicating that our method is also friendly to compression methods that pruning redundant computation.

4.3 Sensitivity study

Impact of Batch Size. Figure 7 presents the latency comparison under different batch sizes. Smaller batches result in higher latency due to poor parallel acceleration. Specifically, a tile (16x16 pixels) is allocated 256 threads, so when the batch size is smaller than 256, the task of constructing matrix M_g cannot be evenly divided into each thread, and smaller workload causes worse parallel acceleration.

Impact of Resolution. We evaluate GEMM-GS on rendering images with various resolutions, from 1x to 3x, as shown in Figure 6. GeMM-GS provides 1.73x and 1.74x speedup over vanilla 3DGS on

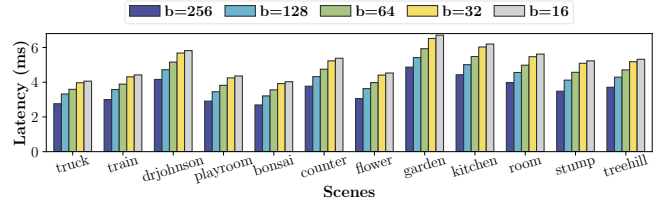


Figure 7: Average rendering latency (ms) comparison between GEMM-GS and vanilla 3DGS with various batch size b.

2x and 3x resolution, emphasizing the scalability of our method on high-resolution scenarios.

5 Conclusion

This paper presents GEMM-GS, an approach to accelerating 3DGS rendering on modern GPUs with tensor cores. By leveraging intra-tile relative coordinates, we propose a GEMM-compatible variant of the 3DGS blending operation that enables acceleration via tensor cores. While TC-GS [15] explores Tensor Core integration for 3DGS, GEMM-GS distinguishes itself through architecture-aware optimizations, including asynchronous data fetch and mini-batch design with PTX-based GEMM instructions. By maximizing GPU hardware utilization, GEMM-GS achieves superior speedups over existing acceleration methods.

References

- [1] Jonathan T Barron, Ben Mildenhall, Dor Verbin, Pratul P Srinivasan, and Peter Hedman. 2022. Mip-nerf 360: Unbounded anti-aliased neural radiance fields. In *Proceedings of the IEEE/CVF conference on computer vision and pattern recognition*. 5470–5479.
- [2] Zhenqi Dai, Ting Liu, and Yanning Zhang. 2025. Efficient Decoupled Feature 3D Gaussian Splatting via Hierarchical Compression. In *Proceedings of the IEEE/CVF Conference on Computer Vision and Pattern Recognition (CVPR)*. 11156–11166.
- [3] Zhiwen Fan, Kevin Wang, Kairun Wen, Zehao Zhu, Dejia Xu, Zhangyang Wang, et al. 2024. Lightgaussian: Unbounded 3d gaussian compression with 15x reduction and 200+ fps. *Advances in neural information processing systems* 37 (2024), 140138–140158.
- [4] Guofeng Feng, Siyan Chen, Rong Fu, Zimu Liao, Yi Wang, Tao Liu, Boni Hu, Linning Xu, Zhilin Pei, Hengjie Li, et al. 2025. Flashgs: Efficient 3d gaussian splatting for large-scale and high-resolution rendering. In *Proceedings of the Computer Vision and Pattern Recognition Conference*. 26652–26662.
- [5] Yu Feng, Weikai Lin, Yuge Cheng, Zihan Liu, Jingwen Leng, Minyi Guo, Chen Chen, Shixuan Sun, and Yuhao Zhu. 2025. Lumina: Real-Time Neural Rendering by Exploiting Computational Redundancy. In *Proceedings of the 52nd Annual International Symposium on Computer Architecture*. 1925–1939.
- [6] Sharath Girish, Kamal Gupta, and Abhinav Shrivastava. 2024. Eagles: Efficient accelerated 3d gaussians with lightweight encodings. In *European Conference on Computer Vision*. Springer, 54–71.
- [7] Alex Hanson, Allen Tu, Geng Lin, Vasu Singla, Matthias Zwicker, and Tom Goldstein. 2025. Speedy-splat: Fast 3d gaussian splatting with sparse pixels and sparse primitives. In *Proceedings of the Computer Vision and Pattern Recognition Conference*. 21537–21546.
- [8] Alex Hanson, Allen Tu, Vasu Singla, Mayuka Jayawardhana, Matthias Zwicker, and Tom Goldstein. 2025. PUP 3D-GS: Principled Uncertainty Pruning for 3D Gaussian Splatting. In *Proceedings of the IEEE/CVF Conference on Computer Vision and Pattern Recognition (CVPR)*. 5949–5958.
- [9] Peter Hedman, Julien Philip, True Price, Jan-Michael Frahm, George Drettakis, and Gabriel Brostow. 2018. Deep blending for free-viewpoint image-based rendering. *ACM Transactions on Graphics (ToG)* 37, 6 (2018), 1–15.
- [10] Bernhard Kerbl, Georgios Kopanas, Thomas Leimkühler, and George Drettakis. 2023. 3d gaussian splatting for real-time radiance field rendering. *ACM Trans. Graph.* 42, 4 (2023), 139–1.
- [11] Arno Knapitsch, Jaesik Park, Qian-Yi Zhou, and Vladlen Koltun. 2017. Tanks and temples: Benchmarking large-scale scene reconstruction. *ACM Transactions on Graphics (ToG)* 36, 4 (2017), 1–13.
- [12] Junseo Lee, Seokwon Lee, Jungi Lee, Junyong Park, and Jaewoong Sim. 2024. Gscore: Efficient radiance field rendering via architectural support for 3d gaussian splatting. In *Proceedings of the 29th ACM International Conference on Architectural Support for Programming Languages and Operating Systems, Volume 3*. 497–511.
- [13] Joo Chan Lee, Daniel Rho, Xiangyu Sun, Jong Hwan Ko, and Eunbyung Park. 2024. Compact 3d gaussian representation for radiance field. In *Proceedings of the IEEE/CVF Conference on Computer Vision and Pattern Recognition*. 21719–21728.
- [14] Haomin Li, Yue Liang, Fangxin Liu, Bowen Zhu, Zongwu Wang, Yu Feng, Liqiang Lu, Li Jiang, and Haibing Guan. 2026. ORANGE: Exploring Ockham’s Razor for Neural Rendering by Accelerating 3DGS on NPUs with GEMM-Friendly Blending and Balanced Workloads. In *2026 IEEE International Symposium on High Performance Computer Architecture (HPCA)*. IEEE, 1–15.
- [15] Zimu Liao, Jifeng Ding, Siwei Cui, Ruixuan Gong, Boni Hu, Yi Wang, Hengjie Li, Hui Wang, Xingcheng Zhang, and Rong Fu. 2025. Tc-gs: A faster gaussian splatting module utilizing tensor cores. In *Proceedings of the SIGGRAPH Asia 2025 Conference Papers*. 1–9.
- [16] Weikai Lin, Yu Feng, and Yuhao Zhu. 2025. Metasapiens: Real-time neural rendering with efficiency-aware pruning and accelerated foveated rendering. In *Proceedings of the 30th ACM International Conference on Architectural Support for Programming Languages and Operating Systems, Volume 1*. 669–682.
- [17] Fangxin Liu, Haomin Li, Bowen Zhu, Zongwu Wang, Zhuoran Song, Haibing Guan, and Li Jiang. 2025. Asdr: Exploiting adaptive sampling and data reuse for cim-based instant neural rendering. In *Proceedings of the 30th ACM International Conference on Architectural Support for Programming Languages and Operating Systems, Volume 3*. 18–33.
- [18] Saswat Subhajyoti Mallick, Rahul Goel, Bernhard Kerbl, Markus Steinberger, Francisco Vicente Carrasco, and Fernando De La Torre. 2024. Taming 3dgs: High-quality radiance fields with limited resources. In *SIGGRAPH Asia 2024 Conference Papers*. 1–11.
- [19] Ben Mildenhall, Pratul P. Srinivasan, Matthew Tancik, Jonathan T. Barron, Ravi Ramamoorthi, and Ren Ng. 2021. NeRF: representing scenes as neural radiance fields for view synthesis. *Commun. ACM* 65, 1 (dec 2021), 99–106. doi: 10.1145/3503250
- [20] K Navaneet, Kossar Pourahmadi Meibodi, Soroush Abbasi Koohpayegani, and Hamed Pirsiavash. 2023. Compact3d: Compressing gaussian splat radiance field models with vector quantization. *arXiv preprint arXiv:2311.18159* 2, 3 (2023).
- [21] Simon Niedermayr, Josef Stumpfegger, and Rüdiger Westermann. 2024. Compressed 3d gaussian splatting for accelerated novel view synthesis. In *Proceedings of the IEEE/CVF Conference on Computer Vision and Pattern Recognition*. 10349–10358.
- [22] Nvidia. 2017. V100 Data Sheet. <https://images.nvidia.cn/content/technologies/volta/pdf/volta-v100-datasheet-update-us-1165301-r5.pdf>.
- [23] Nvidia. 2020. A100 Data Sheet. <https://www.nvidia.com/content/dam/en-zz/Solutions/Data-Center/a100/pdf/nvidia-a100-datasheet-nvidia-us-2188504-web.pdf>.
- [24] Nvidia. 2022. H100 Data Sheet. <https://resources.nvidia.com/en-us-hopper-architecture/nvidia-tensor-core-gpu-datasheet>.
- [25] Nvidia. 2023. H200 Data Sheet. <https://nvdam.widen.net/s/nb5zszsdf/hpc-datasheet-sc23-h200-datasheet-3002446>.
- [26] Nvidia. 2024. B200 Data Sheet. <https://nvdam.widen.net/s/wwnsrxrm2w/blackwell-datasheet-3384703>.
- [27] Panagiotis Papantonakis, Georgios Kopanas, Bernhard Kerbl, Alexandre Lanvin, and George Drettakis. 2024. Reducing the memory footprint of 3d gaussian splatting. *Proceedings of the ACM on Computer Graphics and Interactive Techniques* 7, 1 (2024), 1–17.
- [28] Lukas Radl, Michael Steiner, Mathias Parger, Alexander Weinrauch, Bernhard Kerbl, and Markus Steinberger. 2024. Stoptheop: Sorted gaussian splatting for view-consistent real-time rendering. *ACM Transactions on Graphics (TOG)* 43, 4 (2024), 1–17.
- [29] Jiaming Sun, Xi Chen, Qianqian Wang, Zhengqi Li, Hadar Averbuch-Elor, Xiaowei Zhou, and Noah Snavely. 2022. Neural 3D Reconstruction in the Wild. In *ACM SIGGRAPH 2022 Conference Proceedings (SIGGRAPH '22)*. Association for Computing Machinery, New York, NY, USA, Article 26, 9 pages. doi: 10.1145/3528233.3530718
- [30] Matthew Tancik, Vincent Casser, Xinchun Yan, Sabeek Pradhan, Ben Mildenhall, Pratul P Srinivasan, Jonathan T Barron, and Henrik Kretschmar. 2022. Block-nerf: Scalable large scene neural view synthesis. In *Proceedings of the IEEE/CVF Conference on Computer Vision and Pattern Recognition*. 8248–8258.
- [31] Chen Wang, Xian Wu, Yuan-Chen Guo, Song-Hai Zhang, Yu-Wing Tai, and Shi-Min Hu. 2022. Nerf-sr: High quality neural radiance fields using supersampling. In *Proceedings of the 30th ACM International Conference on Multimedia*. 6445–6454.
- [32] Lizhou Wu, Haozhe Zhu, Siqi He, Jiawei Zheng, Chixiao Chen, and Xiaoyang Zeng. 2024. GauSPU: 3D Gaussian Splatting Processor for Real-Time SLAM Systems. In *2024 57th IEEE/ACM International Symposium on Microarchitecture (MICRO)*. IEEE, 1562–1573.
- [33] Allan Zhou, Moo Jin Kim, Lirui Wang, Pete Florence, and Chelsea Finn. 2023. NeRF in the Palm of Your Hand: Corrective Augmentation for Robotics via Novel-View Synthesis. In *Proceedings of the IEEE/CVF Conference on Computer Vision and Pattern Recognition (CVPR)*. 17907–17917.